ADVANCED FUNCTIONAL MATERIALS
www.afm-journal.de

A Stretchable Highoutput Triboelectric Nanogenerator Improved by MXene Liquid Electrode with High Electronegativity

Wen-Tao Cao, Han Ouyang, Wei Xin, Shengyu Chao, Chang Ma, Zhou Li, Feng Chen,* and Ming-Guo Ma**

Growing demand in intelligent wearable electronics raises an urgent requirement to develop deformable and durable power sources with high electrical performance. Here, a stretchable and shape-adaptive triboelectric nanogenerator (TENG) based on a MXene liquid electrode is proposed. The open-circuit voltage of an MXene-based TENG reaches up to 300 V. The excellent fluidity and highly electronegativity of the MXene liquid electrode, gives the TENG long-term reliability and stable electrical output regardless of diverse extreme deformations. With harvesting mechanical energy from hand tapping motion, the TENG in a self-charging system can charge up capacitors to drive wearable electronics. Moreover, the TENG can be attached to both human skin and clothes as a human motion monitoring sensor, which can inspect the frequency and amplitude of various physiological movements. This work provides a new methodology for the construction of stretchable power sources and self-powered sensors, which have potential applications in diverse fields such as robotics, kinesiology, and biomechanics.

1. Introduction

With the rapid advancement of innovative technology over the past decades, wearable electronics have aroused intense attention because of their tremendous application potential in many fields.[1] Meanwhile, rapid growth of wearable/portable electronics is also accompanied by a great demand for high-performance power sources.[2] Although some promising advances in high-efficient energy harvesters have been gained, the strong dependence on external operating conditions such as sunlight,[3] heat sources,[4] and polarization[5] makes it still a great challenge for their applications as sustainable power sources. As a comparison, harvesting biomechanical energy from human movements is considered to be a reliable and independent approach for providing continuous power.

Triboelectric nanogenerators (TENGs), based on the coupling effects of contact electrification and electrostatic induction, are considered a powerful technology for the efficient conversion of mechanical energy into electricity.[6] Up to now, different types of TENGs have been widely reported owing to the merits of ease of fabrication, lightweight, diverse material options, and high energy conversion efficiency.[7] Remarkable progress on triboelectric self-powered electronics toward various applications such as human-machine interfaces,[8] self-tuning drug delivery,[9] implantable medical electronics,[10] and healthcare monitoring.[11] Among them, single-electrode TENGs with potential merits of simple structure and convenience for carrying are more promising to be applied in skin-mounted electronics.[12] The suitable electrode material is the key factor to guarantee the normal operation of single-electrode TENGs.[13] Liquid electrodes (i.e., liquid metal,[14] physiological saline,[15] and graphene oxide dispersion[16]) with high electron

W.-T. Cao, W. Xin, C. Ma, Prof. M.-G. Ma
Research Center of Biomass Clean Utilization
Beijing Key Laboratory of Lignocellulosic Chemistry
College of Materials Science and Technology
Beijing Forestry University
Beijing 100083, P. R. China
E-mail: mg_ma@bjfu.edu.cn

W.-T. Cao, Prof. F. Chen
Department of Orthopedics
Shanghai Tenth People's Hospital
Tongji University School of Medicine
Shanghai 200072, P. R. China
E-mail: fchen@tongji.edu.cn

The ORCID identification number(s) for the author(s) of this article can be found under https://doi.org/10.1002/adfm.202004181.

Dr. H. Ouyang, S. Y. Chao, Prof. Z. Li
CAS Center for Excellence in Nanoscience
Beijing Key Laboratory of Micro-Nano Energy and Sensor
Beijing Institute of Nanoenergy and Nanosystems
Chinese Academy of Sciences
Beijing 100083, P. R. China
E-mail: zli@binn.cas.cn

Dr. H. Ouyang
Beijing Advanced Innovation Centre for Biomedical Engineering
Key Laboratory for Biomechanics and Mechanobiology
of Ministry of Education
School of Biological Science and Medical Engineering
Beihang University
Beijing 100083, P. R. China

DOI: 10.1002/adfm.202004181

mobility and super deformability have been recently considered as an effective electron collector, which can be combined with the flexible elastomer to construct single-electrode TENGs. However, the limited output performance and complex synthesis process have largely impeded the liquid-electrode based TENGs for further development.

MXenes are an emerging class of 2D transition metal carbides and/or nitrides, which were first reported by Gogosti and co-workers in 2011.[17] To date, MXenes have gained considerable attention in diverse application fields, such as supercapacitors, metal batteries, actuators, and so on.[18] More interestingly, MXenes possess an outstanding metallic electronic conductivity and highly electronegative surface, making it attractive for application in TENGs.[19] For example, Jiang et al. successfully constructed an all-electrospun TENG composed of MXene-based film and silk nanofibers film.[19a] Furthermore, a TENG based on MXene and laser-induced graphene electrode was also reported recently.[19b] However, to the best of our knowledge, there are just a few reports on constructing single-electrode TENG based on MXene dispersion.

Herein, for the first time, we demonstrate MXene-based composite dispersions as highly flexible liquid electrodes in TENG. Cellulose nanofibers (CNFs) with a typical 1D nanostructure derived from the natural wood are selected as a dispersant and interlocking agent to promote the interconnections between 2D MXene nanosheets. By employing elastic silicone rubber as both packaging material and triboelectrification layer, the CNFs/MXene liquid electrode-based TENG (CM-TENG) enabled to work in the single-electrode mode. Owing to the enhanced electron-trapping capacity of MXene nanosheets, CM-TENG can generate an open-circuit voltage (V_{oc}) of ≈300 V, a short-circuit current (I_{sc}) of ≈5.5 µA, and a short-circuit transferred charge (Q_{sc}) of ≈120 nC, suggesting an excellent output performance. Moreover, CM-TENG still displays high electrical outputs under various deformations such as stretching, twisting, and folding. A CM-TENG-based self-charging power system was constructed, which can store the output electricity into the capacitors and then power the electronic devices. Additionally, the CM-TENG can also enable to monitor diverse human movements such as finger bending, arm shaking, and human walking. The outstanding energy harvesting and accurate sensing capability of CM-TENG with superior stretchability demonstrate the development prospect for potential utilization in soft robots, green energy sources, human-machine interaction, and wearable electronics.

2. Results and Discussion

2.1. Preparation and Characterization of CM-TENG

The stretchable and multifunctional CM-TENG was fabricated by injecting a conductive CNFs/MXene dispersion into the sealed silicone rubber capsule, as illustrated in **Figure 1**a and

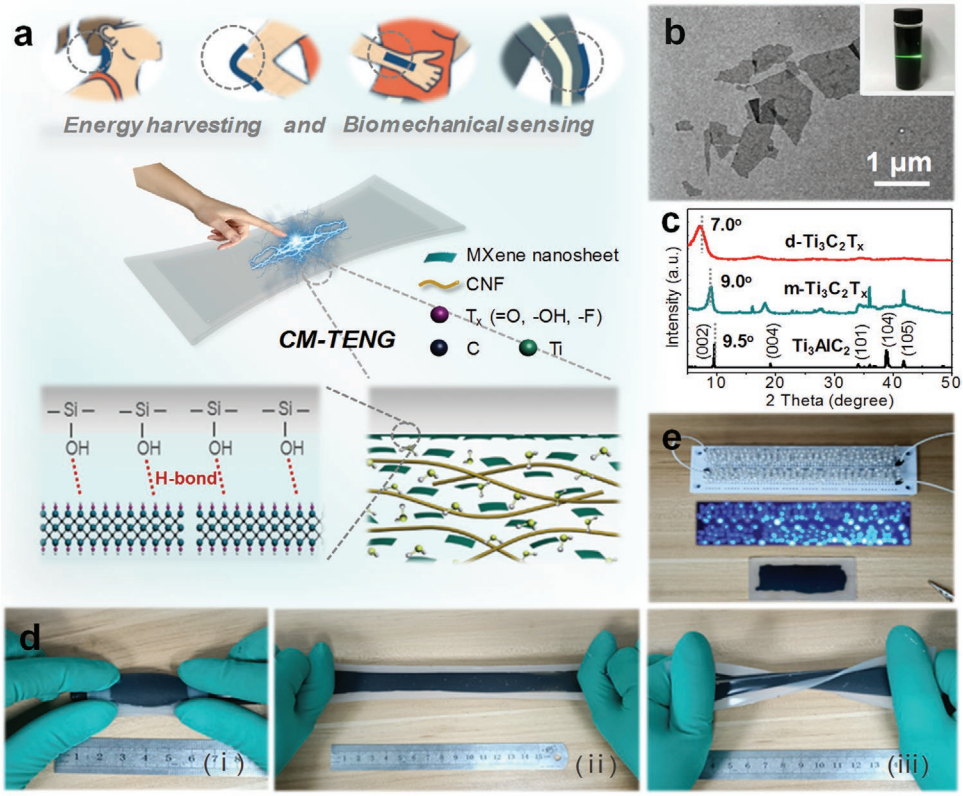

Figure 1. Overview of the stretchable and shape-adaptive CNFs/MXene liquid-electrode based triboelectric nanogenerator. a) Schematic illustration of the CM-TENG for energy harvesting and biomechanical sensing. b) TEM image, and c) XRD patterns of the MXene. The inset picture of (b) is the optical image of d-$Ti_3C_2T_x$ MXene dispersion. d) Photographs of the as-prepared CM-TENG under different mechanical deformations, including i) folding, ii) stretching, and iii) twisting state. e) Photograph of lighting up 230 LEDs by the device.

Figure S1 in the Supporting Information. On the one hand, delaminated $Ti_3C_2T_x$ (d-$Ti_3C_2T_x$) MXene nanosheets were first obtained by a typical chemical exfoliation process from Ti_3AlC_2, as described by Alhabeb et al.[20] Meanwhile, CNFs with a characteristic 1D structure were also extracted from the softwood pulp. Then, the obtained MXene and CNFs can form an evenly mixed dispersion after stirring for 12 h. On the other hand, the silicone rubber was poured into a pre-prepared polytetrafluoroethylene (PTFE) mold. After curing, the silicone rubber film with a rectangular groove was peeled off as the substrate layer. A similar strategy was employed to construct the rough silicone rubber film by using the sandpaper as the template. By inserting a copper wire as the lead wire and then gluing these two silicone rubber layers together, a sealed silicone rubber capsule was acquired. Finally, a CM-TENG can be obtained after the injection of CNFs/MXene mixture into a silicone rubber capsule. This approach makes it easier to develop MXene-based TENGs with excellent stretchability and deformability, increasing their application potential for energy harvesting and self-powered biomechanical sensing.

The d-$Ti_3C_2T_x$ MXene nanosheets were prepared by removing the Al layer from Ti_3AlC_2 precursor (MAX phase) using a mixture of HCl and LiF. The intermediate product, multilayered $Ti_3C_2T_x$ (m-$Ti_3C_2T_x$) MXene, exhibits an accordion-like structure (Figure S2, Supporting Information). The finally obtained d-$Ti_3C_2T_x$ MXene dispersion shows excellent dispersity and stability, reflected by the clear Tyndall scattering effect (Figure 1b). The 2D lamellar structure of MXene nanosheets is observed by the Transmission electron microscopy (TEM) image. Furthermore, the structure evolution from MAX phase to MXene nanosheets can be acquired from the X-ray diffraction (XRD) patterns (Figure 1c). The almost disappearance of the characteristic (104) peak located at $2\theta \approx 39°$ demonstrates the effective removal of Al component. The obvious shift of (002) peak from 9.5° to 7.0°, which is consistent with previous reports,[21] is further confirming the successful fabrication of d-$Ti_3C_2T_x$ MXene nanosheets. CNFs dispersion with an obvious Tyndall scattering effect was prepared from the softwood pulp via a common (2,2,6,6-tetramethylpiperidine-1-oxylradi-cal)-mediated (TEMPO) oxidation method (Figure S3a, Supporting Information). As characterized by TEM measurement, the as-prepared colloidal dispersion contains numerous well-dispersed CNFs with length in the range of 200–600 nm and diameter in ≈20 nm. The Fourier transform infrared (FTIR) spectra reveals the existence of O—H, C=O, and COO— on the surface of CNFs, indicating the successful TEMPO oxidation process (Figure S3b, Supporting Information).

The obtained MXene nanosheets and CNFs can generate a stable mixed suspension after stirring for 12 h, indicating outstanding compatibility between MXene and CNFs in aqueous dispersion (Figure S4a, Supporting Information). The dispersion stability is mainly due to the steric hindrance effect generated by the surface carboxyl groups between CNFs. Besides, the Coulombic-caused mutual repulsion between MXene nanosheets (–24.9 mV) and CNFs (–63.4 mV) can also be a significant factor in promoting the stability of the mixture (Figure S4b, Supporting Information). MXene nanosheets stored in CNFs dispersion generally maintained a stable Zeta potential (≈50 mV) during about 6 months storage (Figure S5a, Supporting Information). In contrast, an obvious weakening of Zeta potential was observed for MXene dispersion, which indicates the attenuation of colloid stability. The MXene dispersion and CNFs/MXene dispersion stored after about 6 months are compared in Figure S5a,b in the Supporting Information, respectively. Visible precipitated clusters of MXene dispersion were observed during the storage. In contrast, the CNFs/MXene dispersion stored for ≈6 months exhibits little color change or aggregation. Additionally, it is well-known that MXene nanosheets have numerous surface functional groups such as –OH, –F, and –O. Thus, CNFs with rich active groups (e.g., –OH, $–COO^-$) can form abundant hydrogen bonds with MXene nanosheets. Moreover, van der Waal interactions between materials may also exist between the materials. Here, the CNFs act not only as a dispersant to guarantee the uniformity of mixed suspension, but also as an interlocking agent to facilitate the interconnections between MXene nanosheets by hydrogen bonding. After injecting the CNFs/MXene mixture into a silicone rubber capsule, a stretchable and shape-adaptive CM-TENG was obtained. The photographs of CM-TENG under diverse deformations demonstrate their excellent foldability, twistability, and stretchability of the devices (Figure 1d). Furthermore, it is found that 230 LEDs connected in series can be lit up simultaneously upon palm tapping the device (Figure 1e and Movie S1, Supporting Information).

2.2. Output Performance of CM-TENG

The electricity generation of CM-TENG is mainly based on the coupling effects of triboelectrification and electrostatic induction, as schematically illustrated in **Figure 2**a,b. Given that plasma-activated silicone rubber film has abundant hydrophilic –OH group, MXene nanosheets with numerous surface terminations (e.g., –OH, –O, and –F) can be absorbed on the activated surface of silicone rubber under the action of hydrogen bonding interactions. Meanwhile, CNFs and water molecules existed in the liquid electrode can also promote the connectivity between MXene nanosheets and silicone rubber. In addition to the conductive CNFs/MXene dispersion that was connected to the floor, the skin was also grounded as human body applied as the ground to construct a single-electrode mode TENG. When human skin contacts with the CM-TENG, owing to the effect of contact electrification, electrons transfer from skin to the surface of silicone rubber and absorbed MXene nanosheets until saturation (state i). Here, silicone rubber film combined with the absorbed MXene nanosheets can be regarded as a triboelectrification layer. MXene nanosheets with higher electron affinity can make the integral triboelectrification layer more "negative," which may cause more electrons inject from skin to silicone rubber/MXene layer. As the skin moves away from the silicone rubber, positive charges are induced in the CNFs/MXene dispersion, leading to instantaneous electrons flow through the external load from the electrode to the ground, forming an electrical signal (state ii). When skin and silicone rubber are separated, the induced positive charges in the CNFs/MXene dispersion would be fully balanced by the negative charges on the surface of silicone rubber, leading to an electrostatic equilibrium (state iii). As the skin approaches the

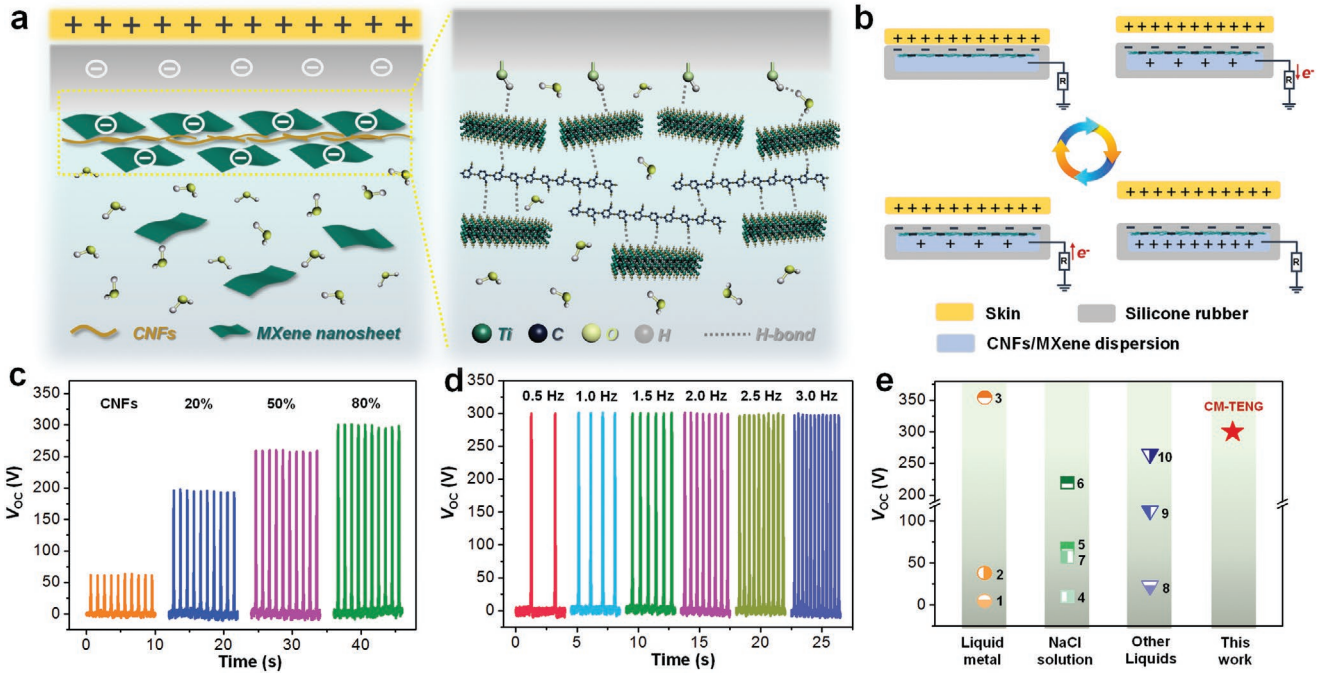

Figure 2. Working mechanism and output performance of the CM-TENG. a) Schematic diagram of the charges distribution of the CM-TENG caused by the contact triboelectrification effect. b) Schematic of the working principle for the CM-TENG. c) V_{oc} of the CM-TENG with various MXene content. d) V_{oc} of the CM-TENG under various operating frequencies ranging from 0.5 to 3.0 Hz. e) Comparison of the output performances of the CM-TENG and the other liquid-electrode based TENGs. The numbers inside (e) are the reference numbers listed in Table S1 in the Supporting Information.

silicone rubber again, the induced positive charges in the liquid electrode get neutralized by the free electrons flowing from the ground, forming a reversed electric output signal (state iv). Thus, repeating the contact-separation movement between the human skin and CM-TENG, an alternating current would be generated. To verify the working mechanism quantitatively, corresponding potential distributions in successive motion steps were simulated by employing COMSOL software, as shown in Figure S6 in the Supporting Information. When the human skin approached or separated from the silicone rubber, the electric potential difference was accordingly changed. Under the action of the changed potential differences, free electrons will be driven to flow to achieve an electrostatic equilibrium. In this process, an alternating current can be produced in the external circuit.

To evaluate the output performance, a commercial PTFE film was employed to simulate human skin as the moving object and contact with the CM-TENG (area, 8×4 cm^2) in cycles by a mechanical linear motor. It is noted that the surface topology structure is an important factor for the output performance of TENG; thus, we developed a template method by molding via sandpaper for fabricating rough surface structures of the silicone rubber film. Figure S7 in the Supporting Information shows the top-view SEM image of the obtained silicone rubber films that were molded using various sandpaper, suggesting an obvious increase in the surface area by introducing numerous microstructures. The relationship between the output performance and the silicone rubber films molded with the different sandpaper was explored (Figure S8, Supporting Information). The results show that the electrical output capacities of the CM-TENG gradually improve with using larger-grit-patterned silicone rubber film as the triboelectric layer. This is mainly due to the larger-grit-molded silicone rubber film have a rougher surface and more air gaps, enabling to increase the contact area and promote the effective separation between two active layers. Moreover, the output performance of the CM-TENG with 320-grit-molded silicone rubber film increase nearly one fold compared to the CM-TENG with untreated rubber film. In this work, the peak V_{oc}, I_{sc}, and Q_{sc} of the CM-TENG can reach 300 V, 5.5 µA, and 120 nC, respectively.

The electrical output performances of the CM-TENG with various d-$Ti_3C_2T_x$ MXene nanosheets content were also systematically investigated. As a convenience, MXene nanosheets-to-CNFs weight ratios were 20:80, 50:50, and 80:20, the resulting CM-TENG are denoted as CM-TENG-20%, CM-TENG-50%, and CM-TENG-80%, respectively. For comparison, the TENG based on CNFs dispersion liquid-electrode (C-TENG) was also fabricated. As shown in Figure 2c and Figure S9 in the Supporting Information, the CM-TENG shows an obvious increase of the electrical outputs compared to that of the C-TENG. It should be ascribed to the electron-trapping ability of MXene nanosheets, which can offer a charge storage layer to increase the electrical outputs. More interestingly, with further increasing the MXene nanosheets-to-CNFs weight ratio to 80:20, the CM-TENG possesses a superhigh voltage output value of ≈300 V, which is about 5 times higher than that the C-TENG. This obvious improvement of output performances indicates that MXene nanosheets play an essential role in promoting the friction charges. Besides, the excellent water dispersibility and abundant surface functional groups of MXene nanosheets will contribute to building hydrogen bonds in water, further accelerating the charge transfer.

Operating frequency is also an important factor in affecting the output performance of the CM-TENG. As illustrated in Figure 2d and Figure S10 in the Supporting Information, when the loading frequency varies from 0.5 to 3.0 Hz, the V_{oc} and Q_{sc} remain basically unchanged at ≈300 V and ≈120 nC, respectively. In contrast, the I_{sc} shows an obvious increase from ≈5.5 to ≈7.8 μA as the operating frequency increases. It is mainly due to that a higher operating frequency can change the contact time between two triboelectric layers and further lead to a higher charge flow rate, which will result in a higher current output eventually. Additionally, the response time of CM-TENG to external force was also characterized, as illustrated in Figure S11 (Supporting Information). The CM-TENG exhibits a supershort response time of about 26 ms at a constant frequency of 2 Hz. The rapid response guarantees the CM-TENG can detect the signal immediately as external force presents. Especially, to verify that the single-electrode CM-TENG can be driven by human skin, the CM-TENG with an area of 8×4 cm^2 was pressed by hand tapping. As illustrated in Figure S12 in the Supporting Information, the CM-TENG can produce a stable electrical output with a peak voltage of ≈350 V at an operating frequency of about 2.5 Hz. In addition, the effect of humidity on the electric outputs of CM-TENG was also explored (Figure S13, Supporting Information). It is observed that the peak output voltage value of the CM-TENG decreases with increasing relative humidity of the environment, and this can be explained by the relative dielectric constant of air increasing with the relative humidity so that the electrical outputs would decrease accordingly. The comfortable relative humidity range for the human body is 45–65% and the CM-TENG could generate detectable electric signals even at ≈70% relative humidity. These results indicate that the CM-TENG could provide suitable responses under daily environment. The superiority of the stretchable CM-TENG over other liquid-electrode based TENGs is highlighted by comparing their output V_{oc} value. As shown in Figure 2e and Table S1 in the Supporting Information, the TENGs based on CNFs/MXene dispersion electrode exhibit higher V_{oc} value when compared with TENGs based on other liquid-electrodes, including liquid metal,[14a,22] NaCl solution,[15a,23] and other liquids.[16,24] The outstanding output performance of the CM-TENG is mainly ascribed to the highly negative surface as well as excellent intrinsic electronic conductivity of the MXene nanosheets.

2.3. Deformability and Durability of CM-TENG

Deformability and durability are significant factors that affect the wearability and lifetime of devices. Thus, CM-TENG was investigated for its capability of producing electricity under various conditions, such as deformations and multiple cyclic contact/separation. As shown in Figure S14 in the Supporting Information, a CM-TENG can be easily and repeatedly stretched 120% with complete elastic resilience. Note that the output performance of CM-TENG under various stretching strain levels, the V_{oc}, I_{sc}, and Q_{sc} first increase and then slightly decrease (**Figure 3**a–c). This performance changes response to the deformation is mainly due to the coupling effect of thickness of the dielectric layer and contacting surface area. When the strain level increase, the silicone rubber would become thinner according to Poisson's effect, as shown in Figure S15 (Supporting Information). The reduction of elastomer's thickness can shorten the distance between surface charges on silicone rubber and CNFs/MXene electrode, resulting in an increase of electrical outputs. Meanwhile, when the device is stretched, the contacting surface area would increase initially and then decrease so that the output performance would change accordingly (Note S1, Supporting Information).[14b] Thus, the increasing trend of the electrical output with increasing the strain level from 0% to 100% can be explained by the positive effects of the greater contacting surface area and thinner silicone rubber layer during stretching. When it was further stretched to 120%, the decrease in output performance is mainly due to the negative effect of the decrease of contacting surface area. Besides, for more challenging tests, the output performances of CM-TENG under other deformations such as twisting and folding were also characterized (Figure S16, Supporting Information). The superior electrical outputs of the device, which recovered from the deformed state, are nearly comparable to the initial value indicate their excellent durability. Moreover, the device at stretching, twisting, and folding state can still drive around 230 LEDs by hand tapping, suggesting the excellent reliability of CM-TENG regardless of extreme conditions (Figure 3f,g and Movie S2, Supporting Information). Figure S17 in the Supporting Information compares the three key aspects: stretchability, peak V_{oc}, and power density of several MXene-based TENGs.[19a-c] Compared with other MXene-based TENGs with limited stretchability, this work first reports a stretchable TENG by employing highly conductive MXene dispersion as the liquid electrode. Especially, MXene nanosheets with highly electronegative surface can be absorbed on the surface of silicone rubber to enhance the electron-trapping capacity of silicone rubber. Thus, CM-TENG with a simple structure can effectively combine the strengths of silicone rubber and MXene to simultaneously realize the outstanding stretchability as well as high output performance.

Additionally, the stability of the CM-TENG was also investigated by the long-term motion cycles, as exhibited in Figure 3d. It can be clearly seen that the single-electrode CM-TENG possesses a stable electrical output capability after ≈6000 cycles of repeated contact-separation motion at a frequency of 2 Hz. Furthermore, the CM-TENG shows no obvious change in output voltage under a 50% strain for 1000 cycles (Figure 3e). As demonstrated above, the excellent mechanical stability of CNFs/MXene dispersion as an electrode facilitates the TENG to satisfy the demands of reliability for practical applications. It should be noted that the single-electrode TENG needs to possess the capability for perceiving different objects in real practical applications. Thus, we selected several common materials such as aluminum (Al), paper, latex, Kapton, and polyethylene terephthalate (PET) to test the electrification capability, while the output voltages of the CM-TENG were recorded, as shown in Figure 3h. Based on the difference of electrification capabilities, there will be different energy generation performance for elastomer contacting with different materials. Importantly, it should be noted that the contact electrification is an extremely intricate process that can be affected by several factors. Not only the intrinsic property of materials but also some

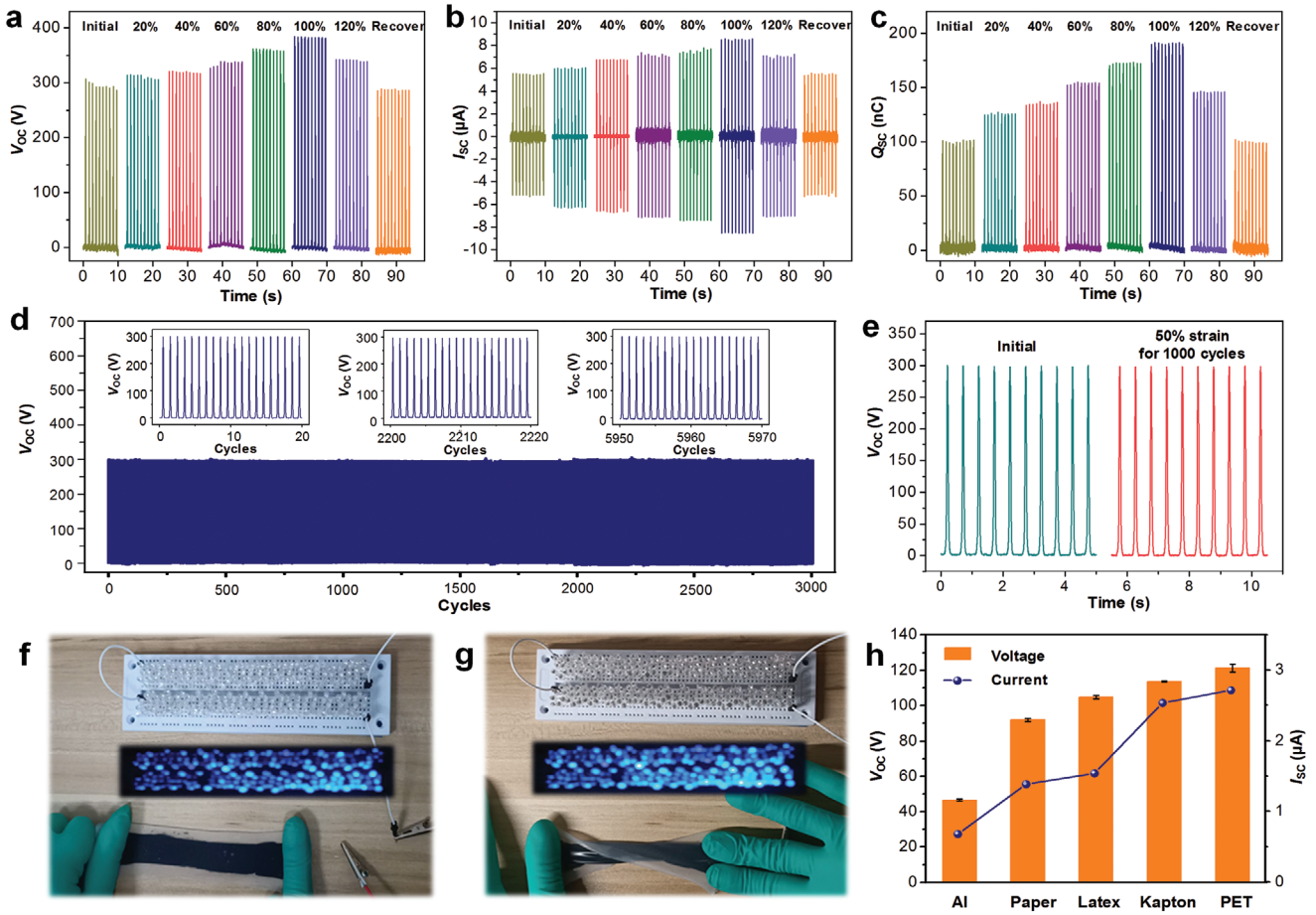

Figure 3. The durability and electrical output characterization of the CM-TENG. Electrical output of the CM-TENG under various stretching strain levels including a) V_{oc}, b) I_{sc}, and c) Q_{sc}. d) Stability and robustness measurement of the CM-TENG, where the V_{oc} was recorded for 6000 cycles at a frequency of 2 Hz. e) Comparison of the V_{oc} of the CM-TENG before and after 50% stretching strain for 1000 cycles. Photograph of lighting up LEDs by the CM-TENG under f) stretching and g) twisting states. h) Generated V_{oc} and I_{sc} of the CM-TENG in contact with different materials.

external factors, such as the stickiness and surface roughness, can all exert an influence on the tribo-induced charges. It was observed that the highest output voltage can be induced by the PET film, while the electrification with Al foil was relatively weak. These experimental results demonstrate that the single-electrode CM-TENG has promising potential for its application under complex surroundings.

2.4. Mechanical Energy Harvesting by the CM-TENG

Based on the outstanding performance of the CM-TENG presented above, we find that the device shows promising potential for energy harvesting. Resistors are employed as external loads to evaluate the output power performance of the CM-TENG. As plotted in **Figure 4**a, the output voltage of the device increased with the resistance increasing from 10^5 to 10^9 Ω. Meanwhile, it is observed that the output current shows a downward trend according to the Ohmic law. As a result, at an external load resistance of 50 MΩ, the CM-TENG can achieve a maximum instantaneous power density value of 504.9 mW m^{-2} (Figure 4b). This delivered power is able to drive some small electronics, addressing the urgent need for sustainable energy supply in a reliable and innovative strategy for the wearable electronics.

To study the capability of the single-electrode TENG as a suitable power source for wearable devices, a CM-TENG based self-charging power system including the commercial capacitor, wearable electronic device, and bridge rectifier was constructed, as displayed in Figure 4c. The CM-TENG was first employed to harvest the mechanical energy, and then the bridge rectifier was used to convert the generated alternative current to direct current, which can further charge the capacitor. The voltages of the commercial capacitors of 22 μF charged by the CM-TENG under different operating frequencies from 0.5 to 3.0 Hz were recorded to evaluate the charging capability (Figure 4d). It can be observed that the charging speed increases gradually as the working frequency increase. The charging curves for diverse capacitors are illustrated in Figure 4e. The charging voltage can reach up to 3 V within 50 s for a 1 μF capacitor, and a 10 μF capacitor was charged to 1.5 V in ≈100 s at a working frequency of 2 Hz. Furthermore, the CM-TENG based self-charging system also possesses a remarkable ability for continuous working (Figure S18, Supporting Information). Besides, the

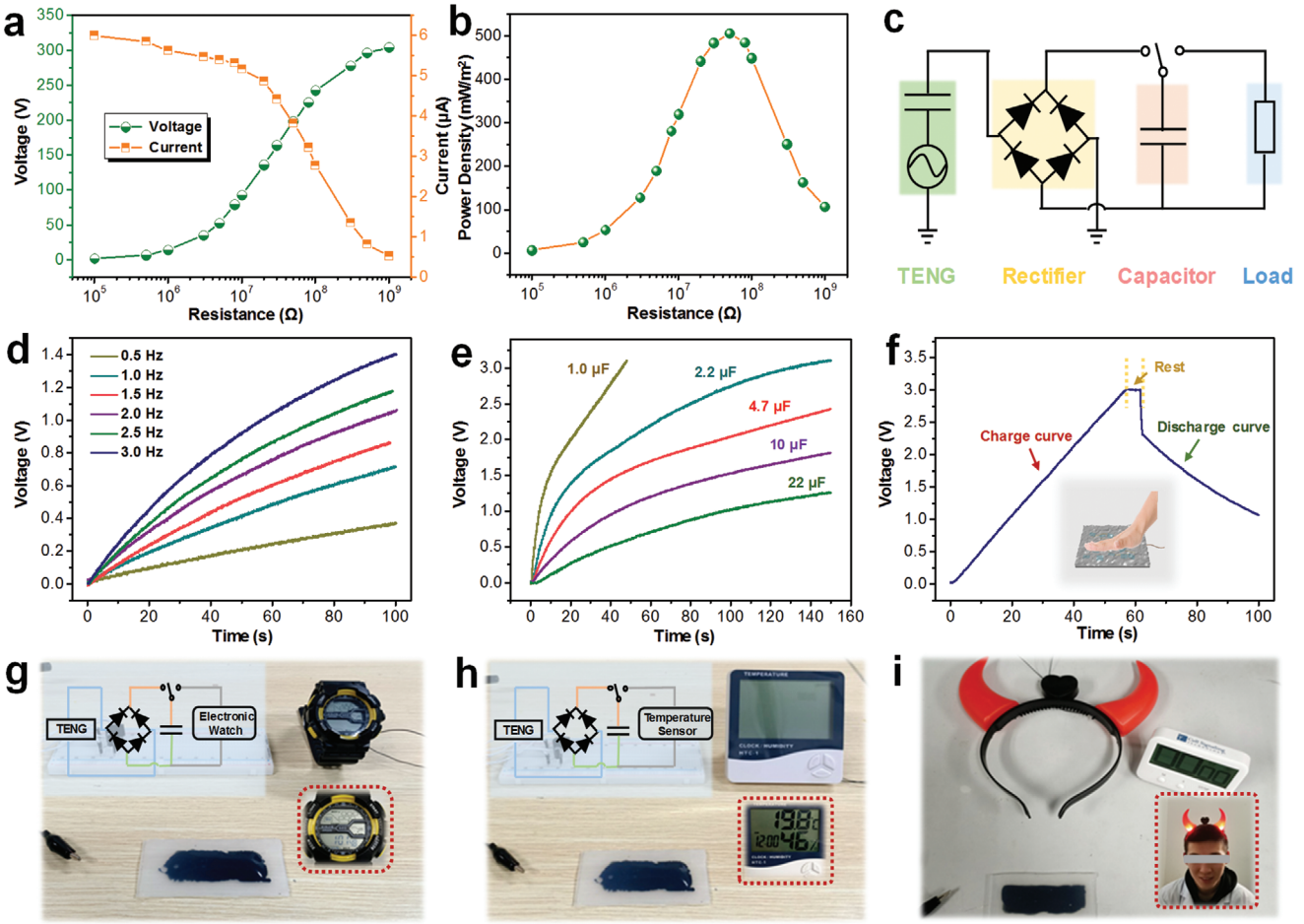

Figure 4. Demonstration of the CM-TENG for biomechanical energy harvesting. a) Output voltage, current, and b) power density of the CM-TENG under various external loads. c) Working circuit of the CM-TENG based self-charging power system. d) Dependence of the charging charge on different working frequencies of the CM-TENG for charging a 22 μF commercial capacitor. e) Charging capability of the CM-TENG under different capacitance capacities (1–22 μF). f) Charging and discharging curves of the capacitor connected on power management. Photographs of the CM-TENG sustainably powering g) an electronic watch, h) a temperature sensor, and i) a luminous hairband.

CM-TENG is capable of harvesting hand tapping energy at a frequency of ≈2 Hz and charge a 10 μF to 3 V in ≈55 s (Figure 4f). Next, we further explored the ability of the CM-TENG based self-charging system to drive commercial electronics directly. As displayed in Figure 4g–i and Movie S3 (Supporting Information), the CM-TENG can harvest sufficient mechanical energy from hand tapping to power an electronic watch, a temperature sensor, or a luminous hairband only rely on a simple circuit, without power management. For example, after harvesting the hand tapping energy for about 60 s, the CM-TENG can drive an electric watch for ≈60 s. Thus, this demonstration suggests that the sustainable CM-TENG based self-powered system possesses enormous potential for deformable and wearable electronics.

2.5. Human Motion Monitoring by the CM-TENG

Stretchability, deformability, and durability are significant attributes of the wearability and portability of devices. Thus, the CM-TENG can be treated as a self-powered biomechanical sensor for monitoring human activities, as demonstrated in **Figure 5** and Movie S4 (Supporting Information). Real-time and continuous human movement detection could provide effective bio-feedbacks for physiological evaluation. For demonstration, the CM-TENG was first mounted on the finger joint of a tester. Figure 5a shows that the cyclic finger bending can be effectively monitored and presented in the form of output voltage signals. Moreover, the peak output voltage value of the CM-TENG would vary with the bending angle. The larger bending angle (90°) of the finger endows the CM-TENG sensor generates higher output peak voltage in contrast to the smaller bending angle (30°). This can be explained by the larger contact area between the silicone rubber and the skin at a larger bending angle. Furthermore, with the finger bending frequency increasing from 0.5 to 1.5 Hz, the maximum output voltage value keeps almost constant (Figure S19, Supporting Information). Nevertheless, the peak number of voltage signal increased from 1 to 3 within 2 s under different bending frequency from 0.5 to 1.5 Hz. The CM-TENG also can identify different pressure generated by finger tapping by recognizing distinguished output voltage signals (Figure 5b). In another case, the CM-TENG sensor could be placed on the wrist joint to monitor

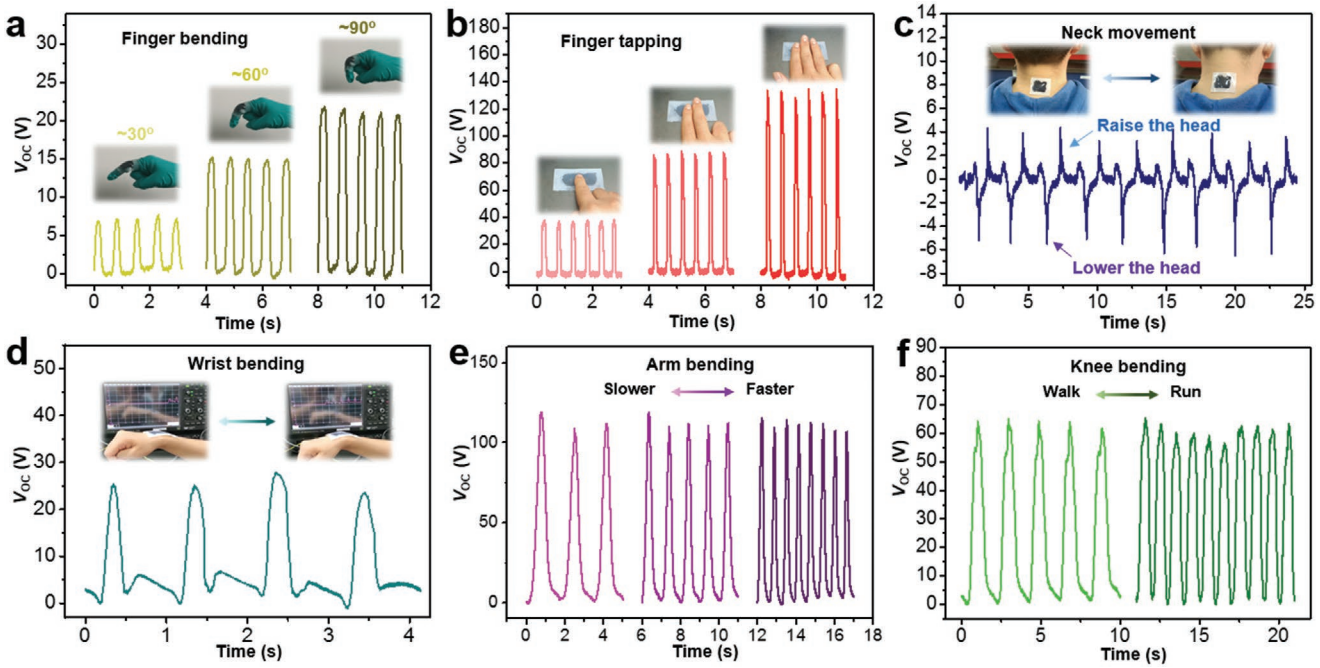

Figure 5. CM-TENG based self-powered biomechanical sensor for monitoring human body movements. Photographs and corresponding V_{oc} of the CM-TENG mounted on finger and neck to monitor a) finger bending, b) finger tapping, and c) neck movement. Generated V_{oc} of the CM-TENG under different bending frequency of d) wrist, e) arm, and f) knee.

the wrist bending movement of a tester. As shown in Figure 5d, the output voltage increased to ≈25 V as bending motion of wrist and decreased to zero as releasing process of wrist. In addition to the body movements with large deformation, the subtle physiological signals can also be captured by the CM-TENG sensor. As depicted in Figure 5c, the CM-TENG was attached to the neck to detect the small deformation of skin and muscle. When the tester raised or lowered the head, the neck movements can be precisely monitored by recording the output voltage signals. Additionally, the real-time signals generated by the CM-TENG subjected to diverse human motions (including wrist bending, arm bending, and knee bending) with different velocity were also measured (Figure 5e,f). With the information acquired from the CM-TENG, we can find that the output voltage signals keep almost constant with the increasing of motion frequency. Meanwhile, the stable electrical output of each bending cycles indicates superior repeatability. Besides, a set of human motion signal collecting and wireless transmission system was also constructed by integrating the CM-TENG and a multi-channels wireless signal transmission module (Movie S5, Supporting Information). The results show that motion signals of wrist bending can be acquired accurately by means of Bluetooth technology. Therefore, the self-powered CM-TENG sensor is capable to monitor the bending angle of the human body joint by analyzing the recorded peak value of electrical output and detect the motion velocity by counting the peak number.

3. Conclusion

In summary, a stretchable and shape-adaptive energy harvester, as well as a self-powered biomechanical sensor based on MXene liquid electrode has been proposed. Working in the single-electrode mode, the CM-TENG with an effective electrode area of 6.0 × 2.5 cm^2 produces the V_{oc}, I_{sc}, and Q_{sc} of 300 V, 5.5 μA, and 120 nC, respectively. The effective combination of soft materials including silicone rubber and MXene-based liquid electrode, guarantees the CM-TENG with excellent electrical output performance under stretched, twisted, and folded deformations. On palm tapping the device, 230 light-emitting diodes connected in series can be easily lit up. Additionally, the CM-TENG with a self-charging system can charge up capacitors to drive several wearable electronics by harvesting energy from hand tapping motion. Especially, by attaching to both human skin and clothes, the CM-TENG can be treated as a biomechanical sensor, which could realize the real-time monitoring of various human motions. This work provides a promising application of MXene-based dispersion as a liquid electrode with high flexibility in constructing multifunctional TENG.

4. Experimental Section

Preparation of d-$Ti_3C_2T_x$ MXene: The d-$Ti_3C_2T_x$ MXene used in this study was prepared by selective etching of Al layers from Ti_3AlC_2 (MAX phase) according to a well-established MILD etching method as reported elsewhere.[20,25] First, 1 g of LiF was dissolved in a pre-configured 20 mL of 9 M HCl by stirring at room temperature. Second, 1 g of Ti_3AlC_2 powder (Jilin 11 technology Co., Ltd) was slowly added to the above HCl/LiF mixture on the condition of constant stirring, and then the reaction continued for 24 h at 35 °C. Third, the resultant suspension was washed with deionized water for several times until its pH > 5, and then the supernatant was decanted. Finally, the collected sediment (multilayered $Ti_3C_2T_x$ MXene) was sonicated under ice bath for 1 h and further centrifuged for another 1 h at 3500 rpm to obtain the d-$Ti_3C_2T_x$ MXene.

Preparation of CNFs: CNFs were prepared based on a common processing method as described previously.[26] Typically, 1 g of softwood pulp was dispersed in 100 mL deionized water containing 0.1 g of NaBr (1×10^{-3} M) and 0.016 g of TEMPO (0.1×10^{-3} M) with constant stirring. NaClO aqueous solution was then added to the above solution dropwise to start oxidization. The oxidized pulp fibers were washed thoroughly with deionized water to get purified. The purified product was then dispersed into nanofibers after vigorous stirring for 20 min. Subsequently, the nanofibers dispersion was centrifuged with a high speed of 10 000 rpm to remove the unfibrillated precipitant. Eventually, the acquired supernatant was treated with a high-pressure homogenizer to obtain the CNFs dispersion.

Fabrication of Stretchable CM-TENG: The stretchable CM-TENG was fabricated by a typical mold casting method. Typically, the liquid silicone rubber (Ecoflex 00–30, V_{Base}:V_{Cure} = 1:1) was first poured into a prefabricated PTFE mold. After precuring at room temperature for 2 h and solidifying at 80 °C for 1 h, the cured silicone rubber substrate was peeled off from the PTFE mold. The rough silicone rubber films were prepared by using the sandpaper with different grits as a template. An oxygen plasma cleaner (IoN 40, PVA TePla) was used to activate one side with smooth surface of the silicone rubber films for 1 min. Two silicone rubber layers were glued together to form a sealed capsule. The conductive liquid was acquired by mixing CNFs and MXene dispersions at different solid content ratio. At last, the CNFs/MXene mixture was injected into the silicone rubber capsule to obtain the flexible CM-TENG.

Characterization and Measurement: The morphologies of the samples were obtained using a JEM-2100F TEM and a field-emission SEM (Hitachi S-4800). An X-ray diffractometer with a Ni-filtered Cu Kα radiation (λ = 1.54178 Å) was performed to obtain the XRD patterns of the samples. FTIR spectra of the samples were recorded on an FTIR spectrometer (FTIR-7600, Lambda Scientific, Australia). A Nano ZS90 laser particle analyzer (Malvern Instruments, UK) was utilized to study the zeta potentials of the samples. The resistance of the liquid single-electrode under various strains was recorded using a CGS-8 Intelligent Sensing Analysis System and a universal mechanical tester (Zwell/roell).

The CM-TENG was driven by a linear motor (Linmot E1100) to realize periodic mechanical traction for electrical measurements. The CM-TENG working under different strain and different frequency was controlled by changing the step distance and step speed of the linear motor. The open-circuit voltage, short-circuit current and transferred charges of the TENG were investigated by a Keithley 6517 electrometer, and the real-time data were acquired and analyzed by an oscilloscope (LeCroy HDO6104).

Supporting Information

Supporting Information is available from the Wiley Online Library or from the author.

Acknowledgements

The authors also thank Professor Zhengwei You and Dr. Lijie Sun for their support. This work is financially supported by the Fundamental Research Funds for the Central Universities (2019YC02), Beijing Forestry University Outstanding Young Talent Cultivation Project (2019JQ03014), the National Natural Science Foundation of China (No. 61875015), the National Postdoctoral Program for Innovative Talent (No. BX20190026), the National Key R&D Program of China (2019YFC1905901), the Key Production Innovative Development Plan of the Southern Bingtuan (2019DB007), the S&T Innovation 2025 Major Special Programme of Ningbo (2018B10040), and the University of Chinese Academy of Sciences. W.X. provided informed consent for their participation in the human experiments and for the publication of the corresponding images and data.

Conflict of Interest

The authors declare no conflict of interest.

Author Contributions

W.-T.C. and H.O. contributed equally to this work. M.G.M., Z.L., F.C., W.-T.C., and H.O. conceived the idea and designed the experiment. M.-G.M., Z.L., and F.C. guided the project. W.T.C. fabricated the TENG. W.T.C., W.X., and C.M., performed the material characterization. H.O. and S.Y.C. carried out the related electrical characterization. W.T.C. and H.O. analyzed the experimental data and prepared the manuscript. All authors discussed and reviewed the manuscript. The figures were updated on December 8, 2020 after initial online publication.

Keywords

energy harvesting, liquid single-electrodes, motion monitoring, MXene, triboelectric nanogenerators

Received: May 14, 2020
Revised: August 3, 2020
Published online: September 13, 2020

[1] a) T. Someya, Z. N. Bao, G. G. Malliaras, *Nature* **2016**, *540*, 379; b) J. Xu, S. H. Wang, G. J. N. Wang, C. X. Zhu, S. C. Luo, L. H. Jin, X. D. Gu, S. C. Chen, V. R. Feig, J. W. F. To, S. Rondeau-Gagne, J. Park, B. C. Schroeder, C. Lu, J. Y. Oh, Y. M. Wang, Y. H. Kim, H. Yan, R. Sinclair, D. S. Zhou, G. Xue, B. Murmann, C. Linder, W. Cai, J. B. H. Tok, J. W. Chung, Z. N. Bao, *Science* **2017**, *355*, 59; c) B. C. K. Tee, J. Y. Ouyang, *Adv. Mater.* **2018**, *30*, 1802560; d) H. Jinno, K. Fukuda, X. M. Xu, S. Park, Y. Suzuki, M. Koizumi, T. Yokota, I. Osaka, K. Takimiya, T. Someya, *Nat. Energy* **2017**, *2*, 780.

[2] a) Y. Shabangoli, M. S. Rahmanifar, M. F. El-Kady, A. Noori, M. F. Mousavi, R. B. Kaner, *Adv. Energy Mater.* **2018**, *8*, 1802869; b) Q. Y. Xia, S. Sun, J. Xu, F. Zan, J. L. Yue, Q. H. Zhang, L. Gu, H. Xia, *Small* **2018**, *14*, 1804149; c) Z. M. Qi, J. L. Tang, S. Misra, C. C. Fan, P. Lu, J. Jian, Z. H. He, V. G. Pol, X. H. Zhang, H. Y. Wang, *Nano Energy* **2020**, *69*, 104381.

[3] a) Y. S. Liu, Y. S. Chen, *Adv. Mater.* **2020**, *32*, 1805843; b) Y. L. Wang, Q. L. Zhu, H. B. Naveed, H. Zhao, K. Zhou, W. Ma, *Adv. Energy Mater.* **2020**, *10*, 1903609.

[4] a) F. Suarez, A. Nozariasbmarz, D. Vashaee, M. C. Ozturk, *Energy Environ. Sci.* **2016**, *9*, 2099; b) H. Choi, Y. Kim, J. Song, C. S. Kim, G. S. Lee, S. Kim, J. Park, S. H. Yim, S. H. Park, H. R. Hwang, M. H. Hong, P. Veluswamy, B. J. Cho, *Adv. Funct. Mater.* **2019**, *29*, 1901505.

[5] a) R. Ding, H. Liu, X. L. Zhang, J. X. Xiao, R. Kishor, H. X. Sun, B. W. Zhu, G. Chen, F. Gao, X. H. Feng, J. S. Chen, X. D. Chen, X. W. Sun, Y. J. Zheng, *Adv. Funct. Mater.* **2016**, *26*, 7708; b) J. Chen, S. K. Oh, N. Nabulsi, H. Johnson, W. J. Wang, J. H. Ryou, *Nano Energy* **2019**, *57*, 670.

[6] a) J. J. Luo, Z. M. Wang, L. Xu, A. C. Wang, K. Han, T. Jiang, Q. S. Lai, Y. Bai, W. Tang, F. R. Fan, Z. L. Wang, *Nat. Commun.* **2019**, *10*, 5147; b) H. Ouyang, Z. Liu, N. Li, B. J. Shi, Y. Zou, F. Xie, Y. Ma, Z. Li, H. Li, Q. Zheng, X. C. Qu, Y. B. Fan, Z. L. Wang, H. Zhang, Z. Li, *Nat. Commun.* **2019**, *10*, 1821; c) X. Y. Li, X. Yin, Z. H. Zhao, L. L. Zhou, D. Liu, C. L. Zhang, C. G. Zhang, W. Zhang, S. X. Li, J. Wang, Z. L. Wang, *Adv. Energy Mater.* **2020**, *10*, 1903024; d) P. Jiang, L. Zhang, H. Y. Guo, C. Y. Chen, C. S. Wu, S. Zhang, Z. L. Wang, *Adv. Mater.* **2019**, *31*, 1902793; e) Y. L. Chen, Y. Zhang,

Z. W. Wang, T. T. Zhan, Y. C. Wang, H. Y. Zou, H. Ren, G. B. Zhang, C. W. Zou, Z. L. Wang, *Adv. Mater.* **2018**, *30*, 1803580.

[7] a) X. Xiao, X. Q. Zhang, S. Y. Wang, H. Ouyang, P. F. Chen, L. G. Song, H. C. Yuan, Y. L. Ji, P. H. Wang, Z. Li, M. Y. Xu, Z. L. Wang, *Adv. Energy Mater.* **2019**, *9*, 1902460; b) Y. C. Lai, Y. C. Hsiao, H. M. Wu, Z. L. Wang, *Adv. Sci.* **2019**, *6*, 1801883; c) Z. Wen, Y. Q. Yang, N. Sun, G. F. Li, Y. N. Liu, C. Chen, J. H. Shi, L. J. Xie, H. X. Jiang, D. Q. Bao, Q. Q. Zhuo, X. H. Sun, *Adv. Funct. Mater.* **2018**, *28*, 1803684; d) Z. Y. Wu, W. B. Ding, Y. J. Dai, K. Dong, C. S. Wu, L. Zhang, Z. M. Lin, J. Cheng, Z. L. Wang, *ACS Nano* **2018**, *12*, 5726.

[8] T. Chen, Q. F. Shi, M. L. Zhu, T. Y. Y. He, L. N. Sun, L. Yang, C. Lee, *ACS Nano* **2018**, *12*, 11561.

[9] Z. R. Liu, J. H. Nie, B. Miao, J. D. Li, Y. B. Cui, S. Wang, X. D. Zhang, G. R. Zhao, Y. B. Deng, Y. H. Wu, Z. Li, L. L. Li, Z. L. Wang, *Adv. Mater.* **2019**, *31*, 1807795.

[10] a) B. Shi, Z. Liu, Q. Zheng, J. Meng, H. Ouyang, Y. Zou, D. Jiang, X. Qu, M. Yu, L. Zhao, Y. Fan, Z. L. Wang, Z. Li, *ACS Nano* **2019**, *13*, 6017; b) D. Jiang, B. Shi, H. Ouyang, Y. Fan, Z. L. Wang, Z. Li, *ACS Nano* **2020**, *14*, 6436.

[11] a) T. Y. Y. He, H. Wang, J. H. Wang, X. Tian, F. Wen, Q. F. Shi, J. S. Ho, C. K. Lee, *Adv. Sci.* **2019**, *6*, 1807795; b) J. H. Wang, T. Y. Y. He, C. Lee, *Nano Energy* **2019**, *65*, 104039; c) J. Sun, A. Yang, C. Zhao, F. Liu, Z. Li, *Sci. Bull.* **2019**, *64*, 1336; d) Z. Li, Q. Zheng, Z. L. Wang, Z. Li, *Research* **2020**, *2020*, 8710686.

[12] a) S. A. Shankaregowda, R. Ahmed, C. B. Nanjegowda, J. W. Wang, S. R. Guan, M. Puttaswamy, A. Amini, Y. L. Zhang, D. J. Kong, K. Sannathammegowda, F. Wang, C. Cheng, *Nano Energy* **2019**, *66*, 104141; b) N. Gogurla, B. Roy, J. Y. Park, S. Kim, *Nano Energy* **2019**, *62*, 674; c) H. J. Guo, T. Li, X. T. Cao, J. Xiong, Y. Jie, M. Willander, X. Cao, N. Wang, Z. L. Wang, *ACS Nano* **2017**, *11*, 856.

[13] a) L. Y. Wang, W. A. Daoud, *Adv. Energy Mater.* **2019**, *9*, 1803183; b) K. Dong, Z. Y. Wu, J. A. Deng, A. C. Wang, H. Y. Zou, C. Y. Chen, D. M. Hu, B. H. Gu, B. Z. Sun, Z. L. Wang, *Adv. Mater.* **2018**, *30*, 1804944; c) L. Y. Lan, T. H. Yin, C. M. Jiang, X. J. Li, Y. Yao, Z. Wang, S. X. Qu, Z. Z. Ye, J. F. Ping, Y. B. Ying, *Nano Energy* **2019**, *62*, 319.

[14] a) S. Wang, L. Ding, X. W. Fan, W. Q. Jiang, X. L. Gong, *Nano Energy* **2018**, *53*, 863; b) Y. Q. Yang, N. Sun, Z. Wen, P. Cheng, H. C. Zheng, H. Y. Shao, Y. J. Xia, C. Chen, H. W. Lan, X. K. Xie, C. J. Zhou, J. Zhong, X. H. Sun, S. T. Lee, *ACS Nano* **2018**, *12*, 2027.

[15] a) F. Yi, X. F. Wang, S. M. Niu, S. M. Li, Y. J. Yin, K. R. Dai, G. J. Zhang, L. Lin, Z. Wen, H. Y. Guo, J. Wang, M. H. Yeh, Y. L. Zi, Q. L. Liao, Z. You, Y. Zhang, Z. L. Wang, *Sci. Adv.* **2016**, *2*, 1501624; b) X. F. Wang, Y. J. Yin, F. Yi, K. R. Dai, S. M. Niu, Y. Z. Han, Y. Zhang, Z. You, *Nano Energy* **2017**, *39*, 429.

[16] Y. H. Wu, Y. Luo, J. K. Qu, W. A. Daoud, T. Qi, *Nano Energy* **2019**, *64*, 103948.

[17] M. Naguib, M. Kurtoglu, V. Presser, J. Lu, J. J. Niu, M. Heon, L. Hultman, Y. Gogotsi, M. W. Barsoum, *Adv. Mater.* **2011**, *23*, 4248.

[18] a) Z. Zhang, S. Yang, P. P. Zhang, J. Zhang, G. B. Chen, X. L. Feng, *Nat. Commun.* **2019**, *10*, 2920; b) J. Orangi, F. Hamade, V. A. Davis, M. Beidaghi, *ACS Nano* **2020**, *14*, 640; c) X. Tang, D. Zhou, P. Li, X. Guo, B. Sun, H. Liu, K. Yan, Y. Gogotsi, G. X. Wang, *Adv. Mater.* **2020**, *32*, 1906739; d) L. H. Yu, Z. D. Fan, Y. L. Shao, Z. N. Tian, J. Y. Sun, Z. F. Liu, *Adv. Energy Mater.* **2019**, *9*, 1901839; e) G. F. Cai, J. H. Ciou, Y. Z. Liu, Y. Jiang, P. S. Lee, *Sci. Adv.* **2019**, *5*, eaaw7956.

[19] a) C. M. Jiang, C. Wu, X. J. Li, Y. Yao, L. Y. Lan, F. N. Zhao, Z. Z. Ye, Y. B. Ying, J. F. Ping, *Nano Energy* **2019**, *59*, 268; b) C. M. Jiang, X. J. Li, Y. Yao, L. Y. Lan, Y. Z. Shao, F. N. Zhao, Y. B. Ying, J. F. Ping, *Nano Energy* **2019**, *66*, 104121; c) Y. C. Dong, S. S. K. Mallineni, K. Maleski, H. Behlow, V. N. Mochalin, A. M. Rao, Y. Gogotsi, R. Podila, *Nano Energy* **2018**, *44*, 103; d) Q. Jiang, C. S. Wu, Z. J. Wang, A. C. Wang, J. H. He, Z. L. Wang, H. N. Alshareef, *Nano Energy* **2018**, *45*, 266.

[20] M. Alhabeb, K. Maleski, B. Anasori, P. Lelyukh, L. Clark, S. Sin, Y. Gogotsi, *Chem. Mater.* **2017**, *29*, 7633.

[21] a) W. T. Cao, F. F. Chen, Y. J. Zhu, Y. G. Zhang, Y. Y. Jiang, M. G. Ma, F. Chen, *ACS Nano* **2018**, *12*, 4583; b) S. Zhao, H. B. Zhang, J. Q. Luo, Q. W. Wang, B. Xu, S. Hong, Z. Z. Yu, *ACS Nano* **2018**, *12*, 11193; c) W. Cao, C. Ma, S. Tan, M. Ma, P. Wan, F. Chen, *Nano-Micro Lett.* **2019**, *11*, 72; d) W.-T. Cao, C. Ma, D.-S. Mao, J. Zhang, M.-G. Ma, F. Chen, *Adv. Funct. Mater.* **2019**, *29*, 1905898.

[22] L. E. Helseth, *Nano Energy* **2018**, *50*, 266.

[23] a) Y. Zou, P. C. Tan, B. J. Shi, H. Ouyang, D. J. Jiang, Z. Liu, H. Li, M. Yu, C. Wang, X. C. Qu, L. M. Zhao, Y. B. Fan, Z. L. Wang, Z. Li, *Nat. Commun.* **2019**, *10*, 2695; b) R. Y. Liu, X. Kuang, J. N. Deng, Y. C. Wang, A. C. Wang, W. B. Ding, Y. C. Lai, J. Chen, P. H. Wang, Z. Q. Lin, H. J. Qi, B. Q. Sun, Z. L. Wang, *Adv. Mater.* **2018**, *30*, 1705195.

[24] a) Z. Q. Yuan, X. Y. Du, H. D. Niu, N. W. Li, G. Z. Shen, C. J. Li, Z. L. Wang, *Nanoscale* **2019**, *11*, 495; b) J. H. Shi, X. P. Chen, G. F. Li, N. Sun, H. X. Jiang, D. Q. Bao, L. J. Xie, M. F. Peng, Y. N. Liu, Z. Wen, X. H. Sun, *Nanoscale* **2019**, *11*, 7513.

[25] F. Shahzad, M. Alhabeb, C. B. Hatter, B. Anasori, S. M. Hong, C. M. Koo, Y. Gogotsi, *Science* **2016**, *353*, 1137.

[26] a) S. L. Dai, Y. L. Chu, D. P. Liu, F. Cao, X. H. Wu, J. C. Zhou, B. L. Zhou, Y. T. Chen, J. Huang, *Nat. Commun.* **2018**, *9*, 2737; b) R. Xiong, H. S. Kim, S. D. Zhang, S. Kim, V. F. Korolovych, R. L. Ma, Y. G. Yingling, C. H. Lu, V. V. Tsukruk, *ACS Nano* **2017**, *11*, 12008.